Brain Research, 615 (1993) 310–327

BRES 18949

Current source density analysis of the hippocampal theta rhythm: associated sustained potentials and candidate synaptic generators

Jurij Brankačk *, Mark Stewart ** and Steven E. Fox

Department of Physiology, State University of New York Health Science Center, Brooklyn, NY (USA)

(Accepted 19 January 1993)

Key words: Rhythmic slow activity; Field potential; Rat; Current source density

Single-electrode depth profiles of the hippocampal EEG were made in urethane-anesthetized rats and rats trained in an alternating running/drinking task. Current source density (CSD) was computed from the voltage as a function of depth. A problem inherent to AC-coupled profiles was eliminated by incorporating sustained potential components of the EEG. 'AC' profiles force phasic current sinks to alternate with current sources at each lamina, changing the magnitude and even the sign of the computed membrane current. It was possible to include DC potentials in the profiles from anesthetized rats by using glass micropipettes for recording. A method of 'subtracting' profiles of the non-theta EEG from theta profiles was developed as an approach to including sustained potentials in recordings from freely-moving animals implanted with platinum electrodes. 'DC' profiles are superior to 'AC' profiles for analysis of EEG activity because 'DC'-CSD values can be considered correct in sign and more closely represent the actual membrane current magnitudes. Since hippocampal inputs are laminated, CSD analysis leads to straightforward predictions of the afferents involved. Theta-related activity in afferents from entorhinal neurons, hippocampal interneurons and ipsi- and contralateral hippocampal pyramids all appear to contribute to sources and sinks in CA1 and the dentate area. The largest theta-related generator was a sink at the fissure, having both phasic and tonic components. This sink may reflect activity in afferents from the lateral entorhinal cortex. The phase of the dentate mid-molecular sink suggests that medial entorhinal afferents drive the theta-related granule and pyramidal cell firing. The sustained components may be simply due to different average rates of firing during theta rhythm than during non-theta EEG in afferents whose firing rates are also phasically modulated.

INTRODUCTION

The hippocampal theta rhythm or rhythmic slow activity (RSA), a large amplitude sinusoidal EEG pattern with a frequency range of 4 to 12 Hz, is one of the most intensively studied EEG phenomena (for reviews see refs. 30, 37, 47, 51). In the rat, the theta rhythm occurs primarily during head and body movements that can be interpreted as changing the rat's perspective on its environment[50]. Only rarely does theta rhythm occur in rats during motionless behaviors[51]. This paper focuses on the neural circuits generating the field potentials of the theta rhythm in the hippocampus.

Current source density (CSD) analysis is a powerful method for locating sources and sinks of membrane current from a set of extracellularly recorded field potentials obtained at different depths[20,31]. CSD profiles constructed from AC-coupled recordings of rhythmic activity are misleading because: (1) they will underestimate currents associated with repetitive monophasic events; and (2) they can impose a time period where current flows appear opposite to the flow of real currents. The underestimation of the magnitude of generators limits the quantitative analysis of membrane currents, and worse, the presence of false generators makes it impossible to determine even the direction of the current flow. It is true even for profiles of evoked potentials that additional data are required to determine if a laminar sink or source is active or passive. Much more data are required to interpret the 'AC' profiles of an EEG rhythm since, at each depth, it must first be determined whether the sinks or the sources are real.

A solution to the problems associated with AC-coupled recordings is to include the DC component. Sustained potentials can make a substantial contribution

Correspondence: S.E. Fox, Department of Physiology, Box 31, State University of New York Health Science Center, 450 Clarkson Avenue, Brooklyn, NY 11203, USA. Fax: (1) (718) 270-3103.

* Present address: Department of Physiology II, Heinrich-Heine-University, Düsseldorf, Germany.

** Present address: Department of Pharmacology, Box 29, State University of New York Health Science Center, Brooklyn, NY, USA.

to recordings of spontaneous brain activity[12,16,21,32]. We report here the results of depth profiles of the hippocampal theta rhythm obtained using DC-coupled recordings in urethane anesthetized rats, and a method for obtaining stable DC-coupled recordings in freely-moving rats.

CSD estimates, in combination with other data, can identify active synaptic sites. Since hippocampal inputs are highly laminated, this leads to straightforward predictions of the anatomical projections involved in theta rhythm generation. This paper presents CSD profiles of the hippocampal theta rhythm in rats anesthetized with urethane and rats running on a wheel. Where possible, the generators that were judged to be real after inclusion of the sustained components in the CSD analyses are identified. Both the known laminar patterns of termination of afferents and the known firing relations to theta rhythm of those afferent populations are considered in suggesting candidate synaptic generators. Some of these results have been presented in preliminary form elsewhere[8,18].

MATERIALS AND METHODS

Acute experiments

Surgery. Male Sprague–Dawley albino rats (370–510 g) were each fitted with a tracheal tube and an intrajugular cannula under ether anesthesia. The ether was gradually replaced with urethane (1.0 g/kg administered as a 20% solution in distilled water). Small supplemental doses of urethane were given, as needed, during the experiments. Animals were held in a Kopf stereotaxic frame and maintained at 37°C with an isothermal heating pad (Braintree Scientific, Braintree, MA) and/or a shielded heating lamp. Sidearms of the tracheal tubes were connected to a source of moisturized air in order to reduce inspissation of pulmonary mucus. Small holes were drilled through the skull and enlarged when necessary with a rongeur. The dura at the base of each hole was carefully removed and the exposed brain was covered with a petroleum jelly – mineral oil mixture.

All implants were made using stereotaxic coordinates[33]. Stimulating electrodes (150 μm nichrome wires, 0.5 mm tip exposure, 1.0 mm tip separation) were placed in the ventral hippocampal commissure (7.7 mm anterior to the interaural line, 6.0 mm dorsal to the interaural line, 0.75 mm ML) and the angular bundle (1.96 mm AP, 6.5 mm DV, 4.5 mm ML). Recording electrodes were filled with 2 M NaCl and had tip impedances of 2–10 MΩ. One electrode ('reference') was fixed near the hippocampal fissure (4.7 AP, 7.0 mm DV, 3.0 mm ML) and a movable electrode was used to make passes in the identical location on the opposite side. Recording electrodes were referred to an indifferent electrode over cerebellum (1 mm diameter glass filled with 2 M NaCl in 3% agar). Stimulating electrode locations were adjusted to give maximal responses at the reference electrode.

Data recording. Signals were amplified with a custom-built low drift DC amplifier. Four evoked field potentials were digitized (10 kHz, Tektronics 5223 digital oscilloscope), and averaged for alternating stimulation of both the ventral hippocampal commissure and the angular bundle. Stimuli (200 ms monophasic capacitatively-coupled constant current pulses, up to 1 mA intensity) were alternated once every 2 s (once every 4 s at each stimulus location) until 4 evoked potentials were collected for each site. The moveable electrode was advanced in 50 μm steps. At least one segment (20.48 s) each of theta and non-theta EEG were collected at each depth along the pass of the movable electrode. These were filtered (20 Hz low pass, Bessel, −24 dB/octave) and digitized at 100 Hz. The data were stored on disk for off-line analysis. Data from 50 to 70 steps were collected on each track.

Chronic experiments

Behavioral apparatus and training. Female Long–Evans rats (200–300 g) were housed individually with access to food ad libitum. Water was available until behavioral training began, after which the rats received water as reinforcement in the testing apparatus and for half an hour after each training session.

The testing apparatus was a box (42 cm D by 38 cm W by 27 cm H) with an open top. A drinking tube, 6 cm above the floor, was attached to one of the side walls. A light and photocell were placed above and below the drinking tube, respectively. A running wheel (35 cm diameter, 11 cm width) was attached to the back wall and a nearby speaker was used to present a 7 kHz tone. The behavioral test apparatus was controlled by a Commodore C-64 computer[26], which also controlled data collection by a Hewlett-Packard 9836A computer system.

Stable recordings of theta and non-theta EEG for each step of the movable electrode were obtained by having animals alternate between periods of running in the wheel (theta EEG) and periods of nearly motionless drinking behavior (non-theta EEG) in a paradigm similar to that of Buzsáki et al.[11]. The rats were water-deprived for 24 h and preoperatively trained to run in a wheel for a set number of turns in order to receive up to three separate drops of water (totalling about 0.2 ml). The behavioral training took place in the same experimental chamber as the experiments.

A specified number of turns of the wheel would trigger the tone, brake the wheel and activate the water delivery system. In order to receive all three drops, separated by a time interval of 2–4 s, the rat had to remain nearly motionless before and during drinking from the tube, keeping its head between the light and the photocell that straddled the drinking tube. Gross movements allowed the light to reach the photocell and thereby inactivated the water application, released the brake of the running wheel and the rat was then required to run on the wheel again. Animals' behavior was shaped to reach a final criterion of 6–8 turns (depending on the running speed) on the wheel.

During 2 days before surgery the animals had ad libitum access to water. Five or more days after surgery the animals were again water deprived for 24 h and tested. Some rats needed one or two sessions for retraining in order to reach the necessary criterion of 6–8 turns of the running wheel.

Surgery. The animals were anesthetized with Nembutal (40 mg/kg i.p.) and held in a stereotaxic apparatus. Pairs of 150 μm diameter varnish-insulated nichrome wires (0.5 mm tip exposure and 1.0 mm vertical tip separation) were implanted both in the ventral hippocampal commissure (7.7 mm AP, 6 mm DV, 0.5 mm ML) to stimulate commissural afferents contralateral to the movable recording electrode, and in the angular bundle (2.0 mm AP, 4.5 mm ML, 6.5 mm DV) to stimulate fibers of the perforant path. Insulation was removed from a 5 mm length of two 175 μm diameter teflon-insulated platinum/iridium (90/10%) wires which were then bent into a right angle loop and positioned over the cerebellum, serving as an indifferent and a ground electrode, respectively. A 3.5 mm diameter hole was drilled in the skull with its center at 6.0 mm AP and 2.5 mm ML. A 175 μm diameter teflon-insulated platinum-iridium (90%/10%) wire, cut square, was placed near the border of the hole and lowered to the depth of the hippocampal fissure. This served as a stationary electrode from which a fixed reference theta rhythm could be recorded. A nylon tube (5.0 mm inner diameter) was fixed above the hole with dental acrylic. A microdrive could be placed in this tube during the time of recording. The movable platinum electrode (about 100 kΩ at 1 kHz, teflon-insulated, F. Haer, Brunswick, ME, modified by cutting off the tip squarely at 25 to 50 μm diameter) was advanced 317.5 μm per turn (0–80 thread). Step sizes for the movable electrode were occasionally one-quarter turns (80 μm), but more typically steps were one-eighth turns (40 μm).

Data recording. During the experiments a thin, lightweight and flexible cable was connected to gold electrode contacts on the

animal's head, permitting unrestricted movement within all parts of the testing apparatus. Four FETs in the headstage were used as source followers to minimize movement artifacts.

One to 5 passes through hippocampus were made in each animal. At each step of the electrode track, data were collected for evoked field potentials, theta EEG and non-theta EEG (see above). Recordings from the stationary and movable electrodes referred to the cerebellar reference were amplified with custom-built low-drift differential DC amplifiers. One 20.48 s continuous segment of theta EEG collected during running, and two 10.24 s segments of non-theta EEG collected during drinking (immediately before and after the running). Evoked potentials were collected during running. Stimulus sites were alternated using the same timing sequence as described for acute experiments. Evoked field potentials and EEG were monitored on the computer display and/or the digital oscilloscope and only artifact-free segments of EEG, recorded during the correct type of behavior were stored on disk. Very slow changes in DC potential could be nulled before or after moving the electrode. Such adjustments were never made during the collection of a complete set of data for a step. In cases of artifacts or obvious DC drift during data collection the whole data set for a depth was rejected and the data collection repeated. Data from 35 to 65 steps were collected on each track.

Histology. After completion of the last electrode track, the electrode was left in the brain and the animals were deeply anesthetized with Nembutal. Anodal currents (5–10 mA for 10 s) were passed through the stimulating electrodes. The rats were perfused transcardially with 0.9% saline and 10% formalin. Coronal frozen sections (40 μm) were cut, mounted and stained with Cresyl violet. The electrode tracks and the tips of the stationary and stimulating electrodes were verified by light microscopy in the Nissl-stained sections.

Data analysis

EEG recordings from the stationary electrode were analyzed for their rhythmic quality by calculating a 'theta score' based on autocorrelations of cosine-windowed epochs of EEG (1.28 s, 128 points) made every 160 ms[46]. A sine wave within the bandpass of the digital filter (4.1 to 12.3 Hz) yielded theta scores that approached 1.0. Pseudorandom analog noise, having a flat frequency spectrum, produced very small values (averaging < 0.05). Theta scores were used to identify rhythmic and non-rhythmic periods of EEG.

Peaks of identified theta cycles were detected, and acceptable theta cycles were those whose periods fell within pre-set time windows (100 to 272 ms) and were associated with an entire EEG segment whose theta score was above 0.35. The positive peak of this fixed reference theta wave served as a trigger for normalizing cycle durations and averaging the theta waves from the movable electrode at each step[19,46]. At least 50 theta cycles were averaged for each depth. Acceptable non-theta EEG points were associated with segments whose theta scores were below 0.25. The change in potential between non-theta and theta EEG conditions was calculated by averaging all non-theta EEG points and subtracting this value from all points on the average theta wave.

Voltage profiles as a function of recording depth were computed from the average evoked potentials and the average theta waves by smoothing them with a three point rolling average of the voltage in depth (weighting factors: 4 for the center point, 3 for each of the adjacent points). Such smoothing was performed twice for *all* profiles in this study to reduce the high spatial frequency noise. Since CSD estimates are computed from the second derivative of the voltage profile they are particularly subject to noise of high spatial frequency[31]. This pattern of smoothing also allowed the equivalent of a weighted seven-point second derivative estimate when the second difference was computed for adjacent data points[20]. An impedance value of 300 ohm-cm[35] was used for computing current source density for both the evoked potentials and the theta rhythm. The impedance was assumed to be homogeneous and isotropic, in spite of the fact that Holsheimer[25] found variations with depth. Holsheimer also showed that these variations had relatively little effect on the CSD estimates. The second differences of the voltage profile were divided by the square of the step size in cm, and by this impedance value to convert them to CSD estimates. Color contour maps were generated by the computer using linear interpolation between points in the data arrays (rows = voltage as a function of time or theta cycle phase; columns = voltage as a function of depth).

For averaging profiles across animals the histologically verified CA1/dentate profiles from different rats were normalized in two sections. The upper portion of the profile was normalized to equalize, across rats, the distance between the CA1 pyramidal cell layer and the hippocampal fissure. The lower portion was normalized to equalize the distance between the fissure and the dentate granule cell layer. The CA1 pyramidal cell layer and the dentate granule cell layer were determined from the peaks of sinks representing the evoked population spikes[2] and the sources representing recurrent inhibition[3,4]. The hippocampal fissure was located from the peak of the AC theta profile[7]. This AC theta peak fell between the distal extremes of the sinks evoked in CA1 stratum lacunosum moleculare and in the dentate molecular layer in response to stimulation of the perforant path. Other strata were identified by the location of well-known evoked sinks at the sites of termination of excitatory afferents.

RESULTS

Four complete profiles were made through the hippocampus in urethane anesthetized rats ($n = 4$). A total of 34 profiles were made in rats running on a wheel ($n = 17$).

Identification of anatomical landmarks with evoked potentials

Vertical passes were made through the hippocampus (areas CA1 and dentate gyrus) with the intention of running parallel to the principal axes of pyramidal and granule cells. The most precise indicator of the depth of the movable electrode was the appearance of evoked responses to commissural or perforant path stimulation. The specific synaptic and action potential contributions to these responses have been well characterized[1–5,9,13–15,29,55]. Current sinks and sources associated with some components, e.g. population spikes, can be precisely localized. Fig. 1 illustrates the appearance of evoked responses to commissural stimulation along one profile, and the process of extracting the current source density (CSD). A dotted line marks the time of the peak of the population spike in CA1 (Fig. 1, left). Plots of the voltage, longitudinal current, and CSD are shown at the right for the indicated time. Such profiles are limited because only a single time point can be shown. It is clear from the display of field potentials at the left that a surface or contour map could be used to present three dimensions.

CSD profiles computed at multiple time points for the data in Fig. 1 (left), are shown in Fig. 2 (top), displayed as a contour map. Fig. 2 (bottom) shows a similar CSD contour map for perforant path responses on the same electrode track. At the right of each plot is a drawing to illustrate the locations of neurons along the pass (stylized Nissl stain on top and stylized Golgi stain on bottom). The most prominent identifiable sinks

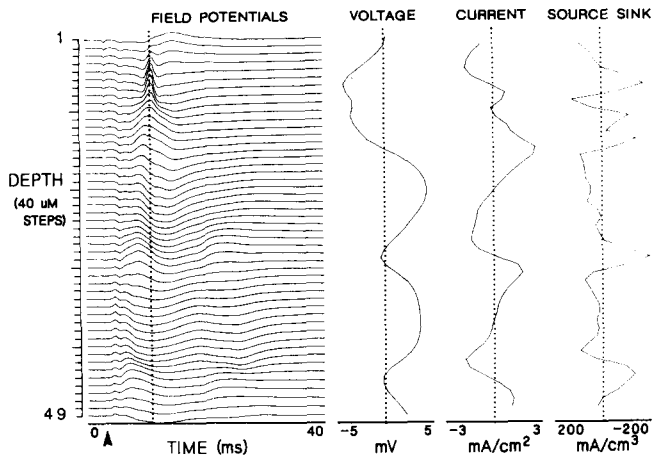

Fig. 1. Field potential responses evoked by stimulation of the ventral hippocampal commissure. At the far left are averaged recordings (40 ms sweep, 4 sweeps per average response) taken at 49 depths through the hippocampus (40 μm intervals). The stimulus occurred 3 ms into the sweep (arrow). The dotted line marks the peak of the population spike at 7.8 ms and is the timepoint for the 3 profiles to the right. The leftmost profile is the voltage as a function of depth. A profile of the first difference of the voltage in depth (proportional to the current flowing in the axis of the profile) is in the middle. Upward currents (with respect to the pyramidal cell layer of CA1) are plotted to the left and downward currents are plotted to the right. The second difference of the voltage in depth (rightmost profile) indicates the density of current appearing in (source) or disappearing from (sink) the extracellular space.

and sources in each plot are lettered and include for Fig. 2A: (a) a sink, at steps 2–3, most probably due to commissural/associational EPSPs on pyramidal cell basal dendrites[1,22]; (b) a sink, at steps 6–8, corresponding to the population spike[2]; (c) a source, at steps 6–8, following the population spike, due to recurrent IPSPs[3,9]; (d) a sink, at steps 10–14, due to commissural/associational EPSPs on pyramidal cell apical dendrites[1,22]; (e) sinks, at steps 28–30 and 43–45, due to commissural/associational EPSPs on granule cells in the dorsal and ventral blades of the dentate gyrus[14]; and (f) sinks, at steps 26–28 and 44–46, presumably due to EPSPs from medial entorhinal afferents[4,13,29]. In Fig. 2B, the response to perforant path stimulation, the most prominent sinks and sources were: (a) a sink, at steps 16–18, due to direct termination of perforant path fibers on CA1 pyramids[5,15,55]; (b) sinks, at 26–28 and 44–47, due to medial perforant path EPSPs in the dorsal and ventral blades of the dentate[4,29,42,43,55]; and (c) sources, at steps 30–32 and 41–43, presumably due to IPSPs on granule cell somata. A granule cell population spike is not obvious in Fig. 2, but appears as an upward extension (into step 42) of the large perforant path sink (Fig. 2B, letter b for the ventral blade of the dentate). Examination of the evoked potential profiles permitted localization of cell body layers and the hippocampal fissure for the profiles of the theta rhythm.

Comparison of AC-coupled and DC-coupled recordings

Fig. 3 illustrates a typical example of the raw EEG field potentials recorded simultaneously in stratum oriens of CA1 (top trace) and stratum moleculare of the dentate gyrus (bottom trace), near the hippocampal fissure in a freely-moving rat. The left side of the figure shows non-theta EEG recorded while the rat was nearly motionless. At the time represented by the middle of the figure the rat started to run in the wheel. A regular 6 to 7 Hz theta rhythm is clear from this point onward. As expected, the theta rhythm recorded from stratum oriens was smaller in amplitude and phase-reversed with respect to the theta rhythm recorded from the molecular layer of the dentate gyrus. Since the methods and equipment were optimized for DC recording, it was possible to observe the sustained potential shifts that were associated with the presence of the theta rhythm (negativity up). In stratum oriens of CA1 the sustained potential shift was small and negative. In the molecular layer of the dentate gyrus the shift was also negative, but was much larger, reaching greater than one millivolt in magnitude. The onset of this sustained potential shift was gradual, requiring 2 s or more to reach a steady level.

Voltage profiles for the EEG are computed the same way as for the evoked potentials except that we used the positive peak of a reference theta wave recorded near the hippocampal fissure as an averaging trigger and normalized the duration of each theta cycle into 8 phase bins. Fig. 4 illustrates the construction of a voltage profile of the theta rhythm and the formation of a three-dimensional plot of the results in a urethane-anesthetized rat. Individual theta cycles from 4 depths are shown to the left, and voltage profiles at 4 points (units are phase, not time) on the theta cycle to the right. A contour map of the surface shown in Fig. 4 (middle) is presented at the top of Fig. 5 (Fig. 5A). Note that, for continuity, two identical copies of the average theta cycle are shown in the contour maps.

Fig. 5B shows CSD as a function of phase and depth for the AC-coupled voltage profile (Fig. 5A). The phase reversal in the voltage profile that occurs in stratum radiatum, the large amplitude of the theta rhythm at the fissure, and the appearance of the CSD profile are similar to results reported in the literature[7,10,11,21,23,54]. Note that at every depth sinks alternate with sources. If, however, DC-coupled recordings of the theta rhythm are used to construct voltage and CSD profiles (Fig. 5C and D, respectively), several differences are obvious. First, there is a DC offset for this voltage profile (Fig. 5C) sufficient to make every point more positive than the indifferent electrode (over cerebellum). Second, the DC potential associated with the theta cycle varies

somewhat with depth. This can be crudely estimated from Fig. 5C by comparing voltages for different depths at about 90 and 270°, when the voltage is near zero in the AC profile (see Fig. 5). The most important difference is apparent in the CSD profile computed from the DC-coupled recordings shown in Fig. 5C. At no depth

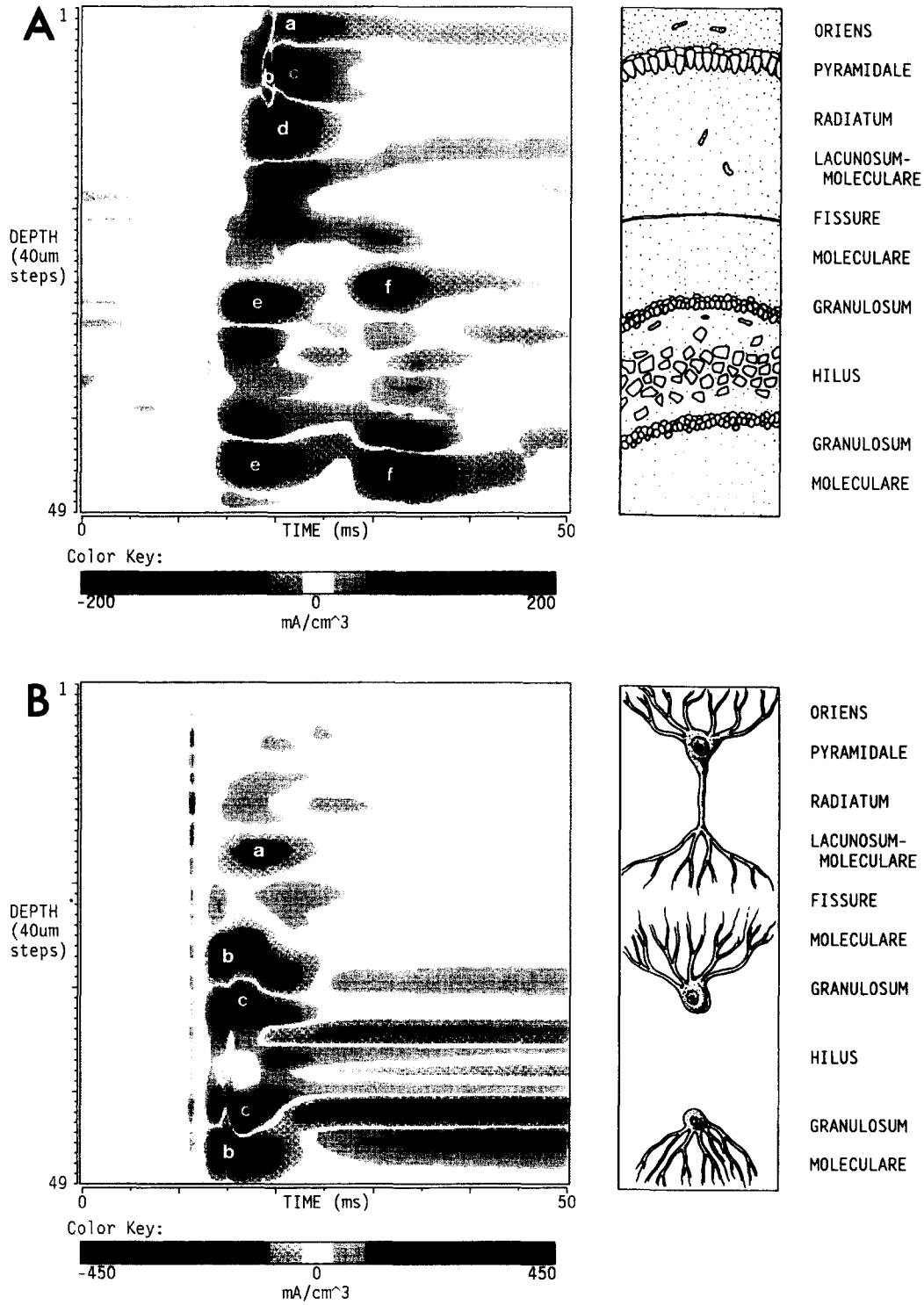

Fig. 2. Contour maps of current source density (CSD) following stimuli to the ventral hippocampal commissure (A) and the perforant path (B) illustrate the utility of evoked responses for identifying anatomical landmarks along the electrode track. Sinks are mapped with colors ranging from green to black. Sources are mapped with colors ranging from yellow-orange to dark brown. Prominent sinks and sources are identified with white lowercase letters. Explanations are in the text. On the right there are drawings of CA1 and dentate gyrus layers, represented at the top like a Nissl-stained pattern and on the bottom as single neurons. The vertical scale of both drawings correspond to the depth scale of the color maps.

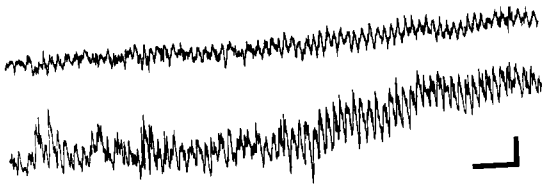

Fig. 3. DC coupled recordings of raw EEG. These were obtained simultaneously from stratum oriens of CA1 (top trace) and stratum moleculare of the dentate gyrus (bottom trace) in a freely-moving rat. At the time represented by the middle of the figure, the rat started to run in the wheel. Negativity is up. Vertical bar: 1 mV; Horizontal bar: 1 s.

do current sinks alternate with current sources. It should be noted that the average theta waves recorded from the fixed reference electrode, including the DC component, were confirmed to be stationary throughout the profile (not shown).

The absolute DC voltage at any point on the profile is of little interest. What matters, for there to be a sink at every phase of the theta cycle at the fissure, for example, is that the *direction* of the curvature of the voltage profile at the fissure be the same at every point on the theta cycle (i.e. that the second derivative of the voltage with respect to depth have the same sign). The DC offset at the fissure is such that the fissure is *more* negative, on every phase of the theta cycle, than the adjacent laminae, but the absolute potential at all nearby points may be positive due to the effects of distant generators. Stratum pyramidale contains only a phasic current source, and stratum oriens contains only a phasic current sink, etc., for similar reasons. Sinks and sources alternate in AC-coupled profiles, at depths where there are relative amplitude maxima (Fig. 5B), because the second derivative of the voltage with respect to depth has one sign when the theta cycle is relatively positive and the opposite sign when it is negative.

Prominent sinks and sources in the DC CSD profile (Fig. 5D) from a urethane anesthetized rat include: (a) a sink, at steps 2–6, in strata oriens and pyramidale of CA1; (b) a source, at steps 6–9, at stratum pyramidale of CA1; (c) a large sink, at steps 13–17, near the hippocampal fissure; (d) a sink, at steps 20–22, in the middle or inner part of the molecular layer of the upper blade of the dentate gyrus; and (e) a source, at steps 23–26, at the level of the granule cell layer of the dorsal blade.

In the AC CSD profile (Fig. 5B), the peaks of large identifiable sources and sinks that were marked in Fig. 5D, are labelled as follows: (a) a sink in stratum oriens peaking at about 20°; (b) a source in proximal stratum radiatum and stratum pyramidale peaking at about 110° after the positive peak of the reference (fissure) theta rhythm; (c) a sink at the fissure peaking at about 155° after the reference theta positive peak; (d) a sink in the middle or inner molecular layer of the dentate gyrus peaking at about 300°; and (e) a source in the dentate hilus peaking between 135° and 170°.

'Difference' profiles in urethane-anesthetized rats

The technical difficulties associated with using pipettes in freely-moving animals led us to develop a method to approach the conditions of Fig. 5C,D without requiring true DC recordings. As indicated in the previous section, the DC potential associated with an average theta cycle varies from lamina to lamina along the axis of the voltage profile. Peak-to-peak variations in CSD profiles of the DC potential associated with theta EEG were about 2.5 times larger than peak-to-peak variations in profiles of the DC associated with non-theta EEG (for the profile in Fig. 5: 18 mA/cm^3 for non-theta and 46 mA/cm^3 for theta). The relatively flatter DC voltage profile of the non-theta was used to construct a 'difference' profile (Fig. 6). The 'difference' profile includes, at each depth, the voltage change from non-theta to theta instead of the actual DC voltage. This means that the DC-coupled recordings need to be stable only for the recording time at each depth, not for the entire electrode pass, to construct a 'difference' profile. Voltage drift and transients that occur between laminae are eliminated, since brief periods of non-theta EEG and theta EEG are recorded at each depth, requiring stability of the recording system (electrodes and amplifiers) for periods of only about 1 min. The 'difference' CSD profile (Fig. 6) is qualitatively very similar to the 'DC' CSD profile (Fig. 5D). A small sink appears in the proximal stratum radiatum (at what was a minimum of a source at this depth in Fig. 5D; see also the level of b in Fig. 5B).

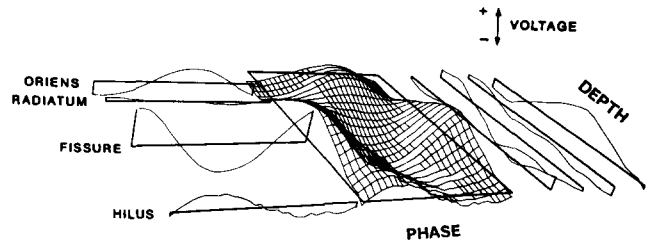

Fig. 4. The process of constructing contour maps from depth profiles of the theta rhythm. At the left are four individual cycles of the AC-coupled theta rhythm from different locations along the profile. Note that the waves at the fissure and in stratum oriens are phase reversed. Note too the amplitude minimum (null) in stratum radiatum. At the right are depth profiles of the voltage at four phases of the theta cycle. Superimposition of the both types of plots creates the surface in the middle of the figure. From such voltage surfaces (and similarly for CSD surfaces) a series of contours are calculated (see Materials and Methods) and color-coded.

'Difference' profiles in freely-moving rats

DC-coupled recordings of the hippocampal EEG were taken using platinum microelectrodes. The testing apparatus was carefully shielded to maximize the stability of the recordings. The stability of the AC component of the reference theta rhythm recorded over the time of the profile was tested for non-stationarity due to factors like systematic changes in theta rhythm amplitude with time or movement of the reference electrode. In chronically prepared rats running on a wheel there was slightly more variability than in urethane-anesthetized rats, but the contribution to the CSD estimates was calculated to be less than 1 mA/cm^3.

Another possible source of noise in the CSD estimates is variability in the amplitude of the AC components of the theta wave recorded from the movable electrode within the period of time required for record-

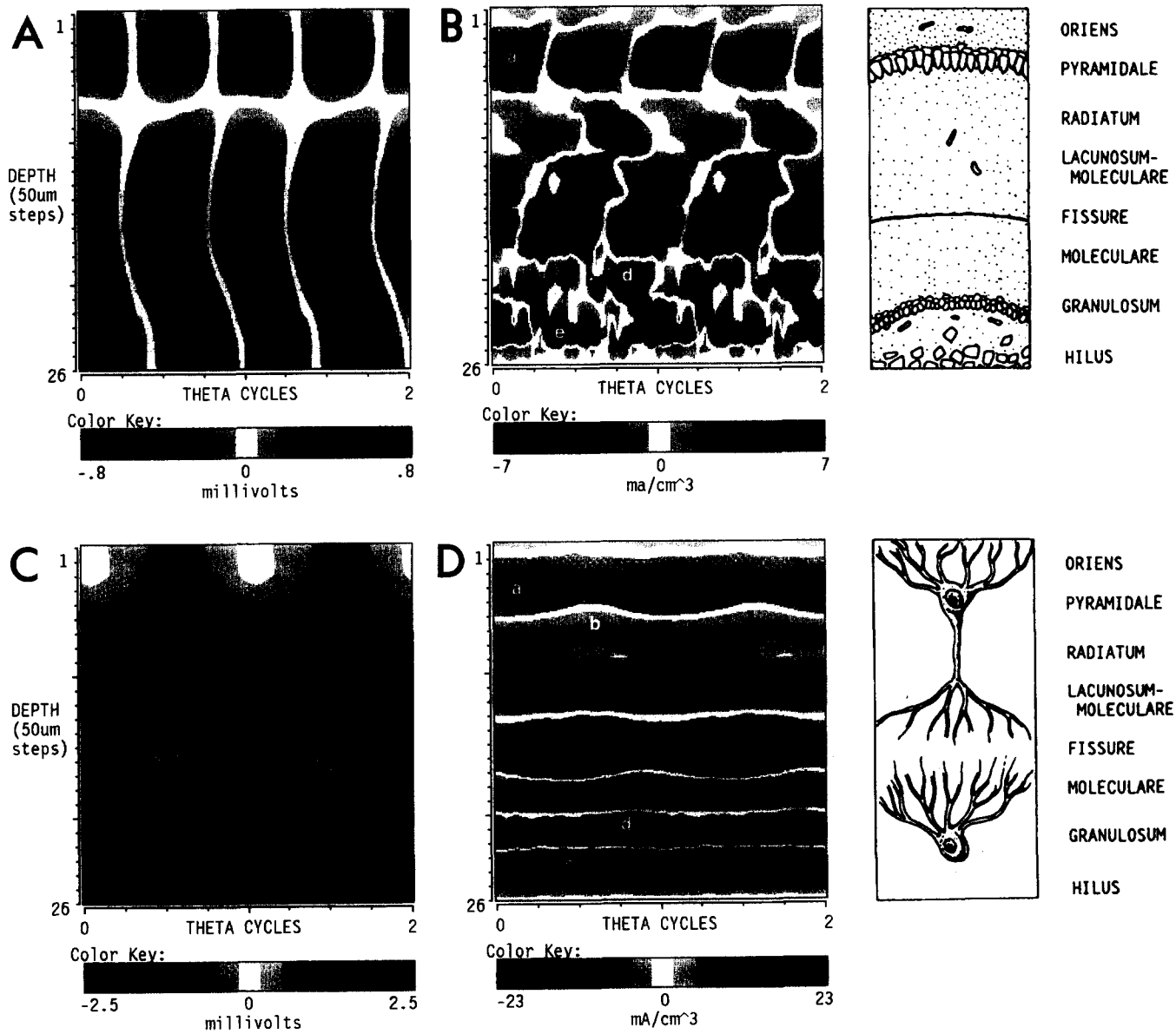

Fig. 5. Contour maps of voltage and CSD profiles of the theta rhythm from a urethane-anesthetized rat contrasting results derived from AC-coupled (A,B) and DC-coupled (C,D) recordings. A: contour map of a voltage profile for AC-coupled theta waves derived from a surface plot such as that in Fig. 4. Note that two copies of the averaged theta cycle are plotted here to emphasize continuity. Cool colors (green through black) represent relatively negative values and warm colors (yellow through brown) represent relatively positive values. The phase shift and null are visible in stratum radiatum. B: CSD contour map derived from the profiles in A. The most prominent feature of this plot is the alternation of sinks and sources at single depths along the profile. C: voltage profile for DC-coupled theta rhythm recordings. The entire profile has a positive offset from the DC recording reference. D: CSD derived from the profile in C reveals sustained and phasic current sinks and sources. In contrast to the AC CSD (shown in B), the DC CSD does not show sinks and sources alternating at single depths, consistent with single afferent systems generating membrane currents at particular depths. Prominent sinks and sources that were seen in all profiles are lettered and described in the text. Scales for color codes are given below each plot.

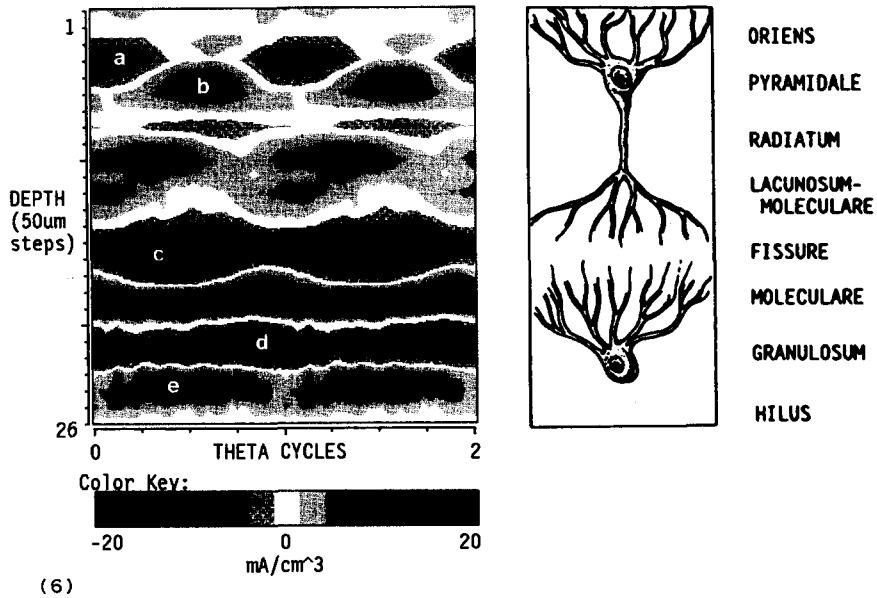

Fig. 6. The 'difference' CSD profile. Depth profiles of the DC potential associated with non-theta EEG (not shown) were judged sufficiently uniform to permit a subtraction procedure where, at each depth, the average DC value of the non-theta EEG was subtracted from the average theta cycle with its DC value. This procedure reduced the requirements for recording stability to the time required to collect a sample of theta rhythm and a sample of non-theta EEG at any depth. The validity of the method was affirmed by the similarity between this plot and Fig. 5D.

ing at one depth in the profile. This could occur due to electrode movement or changes in recording properties of the electrode as a function of time in a particular location. Fig. 7 shows, by comparing results from the first and last halves of the data, that the contribution to the CSD estimates by such noise sources were relatively small (again, less than about 1 mA/cm^3).

A third source of noise in the CSD estimates is due to variability or non-stationarity of the sustained potential component of the theta rhythm and low (temporal) frequency noise. This is a potentially serious source of

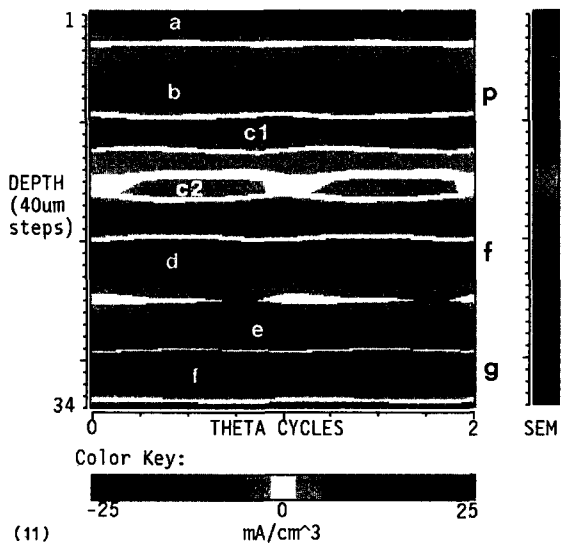

Fig. 11. Average contour map of the current source density estimates of all seven of the histologically verified CA1/dentate profiles from seven different rats normalized to equalize the distances between the CA1 pyramidal cell layer and the hippocampal fissure and between the latter and the dentate granule cell layer. The small white letters identify prominent sinks and sources. CA1 pyramidal cell layer (p), hippocampal fissure (f), dentate granule cell layer (g). The bar on the right indicates the color-coded average value at each depth of the standard error of the mean for these data. This average of the standard error across all phases of the theta rhythm was used here because there was little variation in its value with phase. This also allowed plotting an error figure that occupied only a narrow column. These standard error values indicate that the estimates of the mean value, though variable, are reasonably reliable.

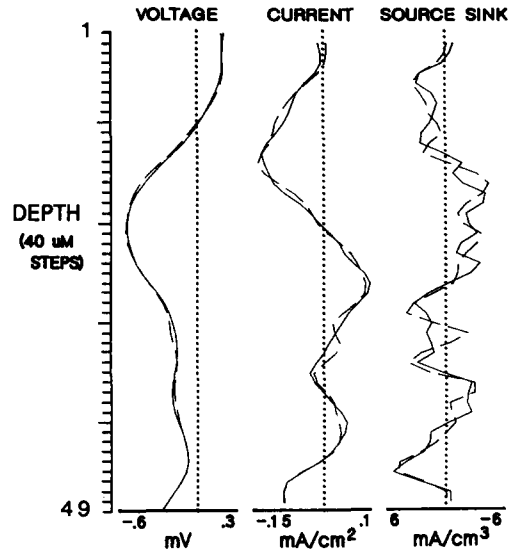

Fig. 7. Variability in profiles of the AC-coupled theta rhythm from a rat running on a wheel. Comparison of profiles constructed using the first half of the recorded data (solid lines) and second half of the recorded data (dashed lines). Left, voltage (theta amplitude at the phase of the positive peak for the theta wave in stratum oriens of CA1) as a function of depth. Middle, first difference of the voltage in depth (longitudinal current). Right, second difference of the voltage in depth (CSD). Axes as in Fig. 1, scales as in Fig. 8, for comparison.

error in locating sources and sinks of current, since the sustained components are large and change dramatically with depth. Recordings of sustained potentials are particularly subject to noise due to environmental factors (e.g. static electricity and changes in contact potentials). Fig. 8 illustrates the variability of the voltage profile of the theta rhythm by comparison of the averages of the first and last halves of the data at each depth. There is substantial disparity in the two voltage profiles. The degree of variation in the first differences of this profile (current flow along the axis of the profile) between the first and last halves, however, is comparable to the variability of the voltage profile. The second differences (CSD) for the first and last half are remarkably similar, considering the degree of difference in the voltage profiles. This suggests that random noise is contributing relatively little to the CSD profiles (usually less than about 15 mA/cm^3). This noise is greater than that of AC profiles, which consequently have greater phase sensitivity. The relatively small variations in the CSD, given the large changes in the voltage profile, illustrate the utility of the current source density calculation for eliminating phenomenological variability in voltage profiles and focusing on the causal processes (sources and sinks of current) in the laminar analysis of field potentials.

At least one of the histologically verified profiles in each of seven rats passed through both the CA1 region of Ammon's Horn and the upper blade of the dentate gyrus. These seven profiles from seven different rats

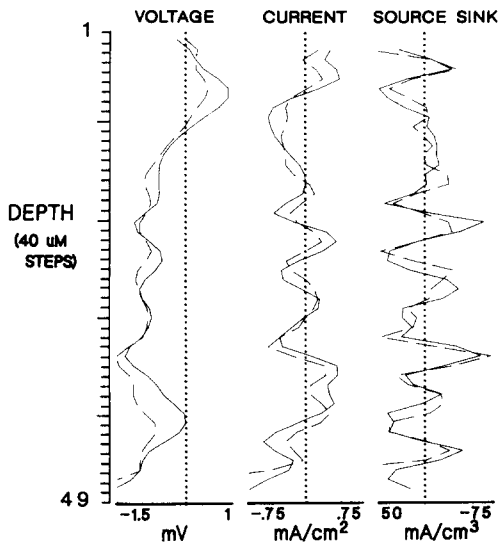

Fig. 8. Variability in profiles of the DC-coupled theta rhythm from a rat running on a wheel (same electrode track as shown in Fig. 7). Profiles computed at the phase of the positive peak of the theta wave in stratum oriens. Data from the first half of the recording (solid lines) and last half of the recording (dashed lines) show greater variability than the AC-coupled data (Fig. 7). Note, however, that these sources and sinks are an order of magnitude greater than those of Fig. 7.

were selected as standard profiles for further analysis. Fig. 9 presents a comparison of voltage and CSD profiles made from AC-coupled recordings (Fig. 9A,B) and 'difference' profiles of voltage and CSD in one of the seven selected profiles. This is the same profile that is illustrated in Figs. 1 and 2. Prominent sources and sinks in Fig. 9D are labelled as follows: (a) a sink, at steps 2–4, in the basal dendrites of the CA1 pyramidal cells; (b) a source, at steps 6–8, at stratum pyramidale of CA1; (c) a sink, at steps 9–16 (divided into two parts by a source in 2/7 cases), in stratum radiatum of CA1; (d) a large sink, at steps 20–22, near the hippocampal fissure; (e) sinks, at steps 26–28 and 44–46, in the middle part of the molecular layer of the upper and lower blades of the dentate gyrus; and (f) sources, at steps 30–32 and 41–43, at the levels of the granule cell layers of the dorsal and ventral blades.

The phases of occurrence of the peaks of the tentatively identified sources and sinks are more easily measured using the AC method. In addition, some phasic components, otherwise obscured by the large sustained components, are discernible only with the AC analyses. In Fig. 9B, the peaks of large sources and sinks for the phasic component of the hippocampal theta rhythm are labelled as follows: (a) a source in stratum pyramidale peaking at about 135° after the positive peak of the reference (fissure) theta rhythm; (b) a sink in stratum radiatum that peaks at about 315°; (c) a sink, not seen in the 'difference' profiles from urethane-anesthetized rats, in stratum lacunosum/moleculare (peak phase about 135°); (d) a sink at the fissure peaking at about 135° after the reference theta positive peak; (e) a sink in the mid-molecular layer of the dentate gyrus peaking at about 270°; and (f) a sink in the proximal molecular layer of the dentate peaking at about 315°.

A phasic sink in stratum oriens of CA1 was not present in the profile shown in Fig. 9B. Such a sink was present in 5 of the 7 selected profiles, but its phase variability was higher than those described above. The mean phase for its peak was 324° ± 59° after the reference theta positive peak. A proximal apical dendritic sink was present at about 0° in CA1 in 4 of the 7 profiles, but neither its location nor its phase were stable across profiles. A pronounced phasic source, at the granule cell layer, was *not* apparent in any of the selected profiles.

The average theta wave *across rats*, using the seven selected CA1/dentate profiles, is illustrated in Fig. 10. In the center is a wireframe three-dimensional surface with depth represented from upper left to lower right. The phase of the average theta wave is represented from lower left to upper right and the 'DC' voltage of

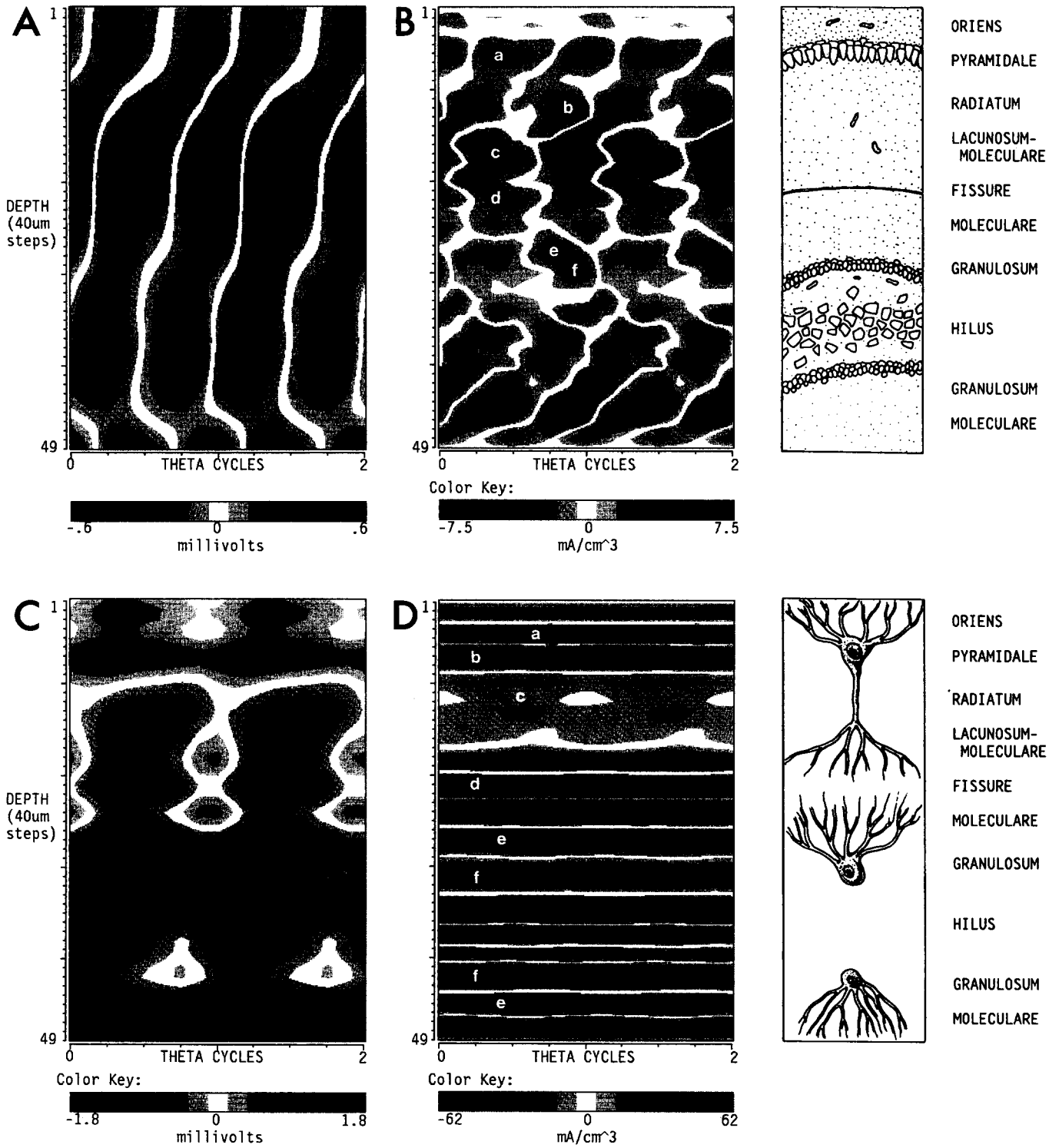

Fig. 9. Contour maps of voltage and CSD profiles of the theta rhythm from a rat during wheel-running illustrate results derived from AC-coupled (A,B) and DC-coupled (C,D) recordings. These data are from the same profile shown in Figs. 1 and 2. A: contour map of a voltage profile for AC-coupled theta waves. Cool colors (green through black) represent relatively negative values and warm colors (yellow through brown) represent relatively positive values. The slower phase shift and amplitude minimum are visible in stratum radiatum (compare with Fig. 5A). B: CSD contour map derived from the profiles in A. Note again the alternation of sinks and sources at single depths along the profile. The profiles in C and D reflect the differences between theta and non-theta; D is comparable to the 'difference' profile in Fig. 6. C: voltage profile for DC-coupled theta rhythm recordings. D: CSD derived from the profile in C reveals sustained and phasic current sinks and sources. Note that the amplitudes for the DC CSD (part D) are more than eightfold larger than the AC CSD (part B). Prominent sinks and sources that were seen in all profiles are lettered and described in the text. Scales for color codes are given below each plot.

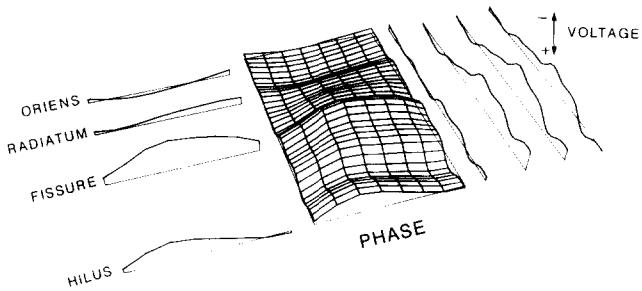

Fig. 10. Three dimensional, perspective view of an DC-coupled 'difference' theta wave. This was averaged across seven rats, taking one CA1/dentate profile for each rat. In the center is a wireframe three-dimensional surface with depth represented from upper left to lower right. The phase of the average theta wave is represented from lower left to upper right. The average value of the 'DC' potential during non-theta EEG is subtracted from the 'DC' voltage of the theta rhythm and this 'difference' is represented from bottom to top (negativity up). No exact voltage calibration is given, because the figure is in perspective, but the peak to peak amplitude of the phasic component of the theta rhythm at the hippocampal fissure averaged about 1.5 mV. On the left, amplitude changes at different phases are shown at selected depths: stratum oriens (ORIENS), stratum radiatum (RADIATUM), hippocampal fissure (FISSURE) and the dentate hilus (HILUS). On the right are cross-sections through the surface taken at selected phases: 0°, 90°, 180° and 270° relative to the positive peak of the dentate theta rhythm near the fissure. Negativity is up.

the theta rhythm is represented from bottom to top (negativity up). On the left these phase and amplitude changes are somewhat more obvious in cross-sections through the surface taken at selected depths. Here it is easy to see, in addition, that the phase shift is gradual in stratum radiatum of CA1[54]. On the right are cross-sections through the surface taken at selected phases. In these it is clear that the field potentials of the theta rhythm change dramatically as a function of depth at all phases of the cycle. Similar voltage profiles for individual animals can be subjected to one-dimensional current source density analysis at each phase point.

Current source density of the theta rhythm computed after normalizing depth and averaging the EEG and sustained potentials in the seven selected profiles is shown in Fig. 11. All of the generators (sources or sinks) shown here are real in the sense that they are not artificially induced by AC coupling. Some of these are active and some are passive. The tentatively identified active sources and sinks in Fig. 11 are labeled as follows:

(a) A sink at steps 1 to 3 in the basal dendrites of the CA1 pyramidal cells. This could be due to EPSPs from either commissural/associational or septal afferents. The fact that this sink is not phasic is in good agreement with the findings of the AC CSD analysis, where it was highly variable in phase, when present at all. This sink is also illustrated in single profiles and marked as 'a' in Figs. 5D (urethane) and 9D (wheel-running).

(b) A source at steps 6 to 9 at the level of stratum pyramidale of CA1. This could be due to somatic IPSPs. It is also illustrated as 'b' in Fig. 9D. It is not apparent under urethane anesthesia (Fig. 5D).

(c1,c2) Two sinks at different depths within stratum radiatum (at steps 10–12 and 15–16). This separation of two sinks by a source also occurred in stratum radiatum of two of the individual wheel-running theta profiles. These two sinks are marked 'c' in Fig. 9D. In urethane anesthesia, stratum radiatum shows a source (see Fig. 5D).

(d) A large sink at steps 20 to 24 near the hippocampal fissure. This could occur due to EPSPs from lateral entorhinal afferents to the distal apical dendrites of both CA1 pyramids and dentate granule cells. In one of the selected profiles the sink appeared only on the dentate side of the fissure. This sink is also prominent in the single profiles. It is marked as 'c' in Fig. 5D (urethane) and as 'd' in Fig. 9D (wheel-running).

(e) A sink at steps 26 to 29 in the middle part of the molecular layer of the dentate gyrus. This is probably due, at least in part, to EPSPs from medial entorhinal afferents. Similar sinks also appeared in the ventral blade of the dentate in 4 of the 5 selected tracks that reached that level. This sink is marked 'e' in Fig. 9D (wheel-running). It may correspond to the sink labeled 'd' in Fig. 5D (urethane), but the latter sink appears to be more proximal to the granule cell layer.

(f) A non-phasic source at steps 30 to 33 at the level of the dentate granule cell layer. These may be caused, at least in part, by somatic IPSPs. Similar sources also appeared in the ventral blade in 5 of the 5 selected tracks that reached that level. The fact that this source is not phasic is in good agreement with the findings of the AC CSD analysis, where phasic somatic sources were not generally discernible. This source is labelled 'e' in Fig. 5D (urethane) and 'f' in Fig. 9D (wheel-running).

The hilar sources and sinks are more variable across rats than those described above. They are also difficult to identify with particular afferents because of the anatomical heterogeneity of the hilar area. The apical dendritic sources in both CA1 and the dentate gyrus

TABLE I

Identification of sources and sinks at the various laminar locations in the hippocampus

Name of stratum	*CSD type*	*Presumed event*	*Presumed afferent*	*VHC latency*	*PP latency*	*AC Θ CSD peak peak*	*DC Θ CSD*
CA1 oriens	sink	EPSP	comm/assoc [a]	7.4 ± 3.0 [b] (6 of 6)	–	324 ± 59° [c] (5 of 7)	no peak (7 of 7)
CA1 pyramidale	sink	pop spk	–	6.0 ± 1.2 (3 of 7)	–	–	–
	source	IPSP	interneurons	6.8 ± 1.3 (7 of 7)	–	145 ± 26° (7 of 7)	145° (5 of 7)
CA1 proximal radiatum	sink	EPSP?	?	–	–	0 ± 73° (4 of 7)	0° [d] (2 of 7)
CA1 radiatum	sink	EPSP	comm/assoc	4.3 ± 0.7 (7 of 7)	10.9 ± 0.8 [e] (6 of 7)	276 ± 28° (7 of 7)	180° (7 of 7)
CA1 lacunosum-moleculare	sink	EPSP	mec & lec	–	4.2 ± 0.7 (5 of 7)	129 ± 31° (7 of 7)	–
Near hippocampal fissure	sink	EPSP?	lec?	–	–	158 ± 39° (7 of 7)	158° [f] (7 of 7)
Dentate mid-moleculare	sink	EPSP	mec	15.9 ± 5.8 (6 of 7)	1.8 ± 0.4 (7 of 7)	260 ± 26° (7 of 7)	300° [g] (7 of 7)
Dentate inner-moleculare	sink	EPSP	comm/assoc [a]	3.1 ± 1.0 (7 of 7)	7.5 ± 1.0 (3 of 7)	334 ± 22° (6 of 7)	–
Dentate granulosum	sink	pop spk	–	–	3.1 ± 0.1 (2 of 7)	–	–
	source	IPSP	interneurons	–	4.4 ± 0.7 (7 of 7)	–	no peak (7 of 7)

[a] In the CSD of the theta rhythm, these sinks (marked 'a' and labeled 'comm/assoc') may also be due to activity in afferents from the medial septal nuclei. Abbreviations for this column are: comm/assoc, commissural and associational afferents; mec, medial entorhinal cortex; lec, lateral entorhinal cortex;

[b] All latencies are expressed in milliseconds to onset.

[c] Phase of the peak of the source or sink relative to the positive peak of the theta rhythm recorded at the hippocampal fissure.

[d] In the DC CSD this sink was usually combined with the CA1 radiatum sink in the row below.

[e] This sink is produced by activation of the 'trisynaptic pathway' from entorhinal cortex to dentate to CA3 to CA1 (Andersen *et al.*[5]).

[f] In two of these seven profiles this sink appeared only on the dentate side of the hippocampal fissure.

[g] In the DC CSD this sink was combined with the dentate inner-moleculare sink in the row below.

are presumed to be entirely passive in the absence of substantive evidence to the contrary. The bar on the right of Fig. 11 indicates the color-coded average value at each depth of the standard error of the mean for these data.

The sources and sinks of current that were observed at different depths within the hippocampal formation in rats running on a wheel are summarized in Table I. Data are presented both for evoked sources and sinks and for those associated with the theta rhythm. Sinks that occur at depths known to have primarily excitatory afferents are presumed to be EPSPs. Sources that occur at depths known to have primarily inhibitory afferents are presumed to be IPSPs. The average onset latencies of each sink or source in the seven selected profiles is given for stimulation of both the ventral hippocampal commissure (VHC Latency) and the perforant path (PP Latency). The frequency of occurrence of each of the sources or sinks in the set of seven selected profiles is given in parentheses. At the level of the cell layers, both sinks associated with population spikes (pop spk) and sources associated with recurrent inhibition were recorded, so these layers have two rows. The peak phases of the sources or sinks are given for the AC and DC CSD analyses of the theta rhythm (AC Θ CSD Peak and DC Θ CSD Peak, respectively) along with their frequency of occurrence (in parentheses) for the seven selected profiles recorded from seven rats during wheel-running.

DISCUSSION

Single electrode voltage profiles were made for the hippocampal theta rhythm in urethane-anesthetized and freely-moving rats. Glass micropipettes permitted stable recordings, including the DC component, of the theta rhythm in anesthetized rats. It is shown that inclusion of the DC component changes the appearance of the current source density profile dramatically. A method was derived from the DC-coupled recordings from anesthetized rats that makes it possible to include sustained potentials in profiles taken from freely-moving rats using metal microelectrodes. The method includes a measure of the 'DC-shift' from non-theta to theta EEG states, and requires stability in

the recording system for periods of only about 1 min at each recording depth. Profiles that include sustained potentials associated with the theta rhythm eliminate one of the major problems of 'AC' profiles. 'AC' profiles constrain the CSD to have extracellular current sinks alternate with sources at most depths. This limits the utility of such profiles for identifying even the direction of a postsynaptic response to activity in an afferent system. Sinks and sources do not alternate at a single lamina in the profiles based on recordings that include the sustained potentials.

Profiles of the sustained potentials associated with the theta rhythm as a function of depth have been reported for curarized rats[21]. We have made depth profiles of the sustained potentials for non-theta and theta EEG in urethane anesthetized rats and depth profiles of the 'DC shift' between non-theta to theta EEG states in freely-moving rats. 'AC' profiles from both preparations are presented for comparison with 'DC' profiles and with previously published reports[7,11,21,23,54]. In comparing the two types of profile, the 'DC' profiles gave the most accurate report of the nature of inputs to a given lamina (magnitude and direction), whereas the 'AC' profile was best for identifying the phase and depth of the peak current (once the correct direction can be selected).

The method developed to permit inclusion of sustained potentials in recordings from rats during wheel-running emphasizes the utility of the non-theta EEG state as a 'control' condition. Studies of single unit activity compare the firing rates and patterns of the cells between the non-theta and the theta EEG states. Likewise, evoked potential analyses across EEG states have examined population-based changes in excitability. Emphasis on activity changes related to the EEG state change permits certain studies such as the CSD reported here and is essential for making comparisons across preparations such as urethane-anesthetized and running rats. The use of the 'difference' in DC potential between non-theta and theta states made it possible to use the platinum electrodes in freely-moving rats. Comparison of the first and last halves of the data showed that the platinum electrodes are sufficiently stable to record a sequence of drinking, then wheel-running, then drinking at a single depth without too much drift. They are not sufficiently stable in moving between steps to obtain true DC values. It should be noted, however, that the relative flatness of the DC voltage profile during the non-theta state has been established here for urethane anesthetized rats. It is only an assumption that this is also the case in freely-moving rats. Our best evidence that this is the case is the similarity of 'difference' profiles of the theta-related CSD in urethane-anesthetized and freely-moving rats.

Assumptions of the current source density analysis

In these studies the current source density (CSD) analysis was performed in one dimension (depth) both for evoked field potentials and for cycles of the theta rhythm. Two important points were considered in selecting the one-dimensional CSD method. First, the location of the recording electrode track was restricted to the section of the hippocampal formation where the cell layers approach the ideal condition of forming a horizontal plane. This allowed the effects of tissue curvature to be neglected in performing the CSD calculations. Second, the paths of electrode penetration were normal to the hippocampal surface. Electrodes were advanced along the axis of symmetry of a synchronously activated sheet-like population of hippocampal neurons, minimizing extracellular current flow normal to the recording dimension.

Others have shown that there is little change in theta rhythm with electrode movement along the septotemporal or transverse axes of the hippocampus[23]. This is a necessary condition for performing a one-dimensional CSD analysis. The currents flowing normal to the axis of electrode penetration must be negligible. Inhomogeneity of tissue conductivity must also be considered. Holsheimer[25] has shown that there are variations in the conductivity of the hippocampus with depth. He measured conductivity and compared CSD estimates that took into account the actual values of the conductivity with those which did not. He found only minor changes in the estimated magnitudes of sources and sinks due to inhomogeneity. No changes in tissue conductivity were included in the CSD analyses presented here.

AC CSD analysis of the theta rhythm

The AC voltage profiles of the theta rhythm reported here corroborate the work of others[7,23,54]. Buzsáki et al.[11] described a phase shift of the theta rhythm that occurs upon entry into the dentate hilus. In our recordings from freely-moving rats, the additional phase shift appeared to be somewhat more superficial than the hilus, occurring in the inner one-third of the dentate molecular layer. The AC CSD analysis results were remarkably similar to those reported by Buzsáki et al.[10]. Our AC CSD profiles of the theta rhythm found the same set of sources and sinks.

Interpretation of AC CSD profiles can be difficult. As noted by Buzsáki et al.[10] the pattern of sources and sinks on opposite phases of the theta rhythm were almost exact 'mirror images', that is, regions that were

sinks become sources and vice versa. At every depth, false sources are introduced by the AC-coupling at the phase of the theta rhythm opposite the peak of the real sinks. Likewise, false sinks are introduced on the phase opposite the real sources. In no case do false sinks or sources appear in the DC CSD profiles, as shown in part D of Figs. 5 and 9. The fact that the DC analysis shows a source or sink to be real, as opposed to false, has no impact on the decision regarding its 'active' or 'passive' nature. Finally, non-phasic sinks and sources do not appear at all in the AC CSD profiles.

On the other hand, the AC CSD analysis did have an advantage. It was more accurate than the DC CSD analysis for determining the depths and phases of occurrence of the peaks of the phasic sources and sinks. This is important both for the identification of afferent populations that may be responsible for the generators and for the comparison of the CSD data with the phase histograms of cells in those afferent populations. There are two reasons for the greater accuracy of the AC CSD of the theta rhythm. First, the AC CSD analysis has a relatively low noise level. As reported in the Results, the noise figures for DC theta-related CSD estimates are an order of magnitude or more higher than those for AC estimates. Secondly, if sustained generators are caused by different mechanisms than phasic generators, they may peak at different depths. Superposition of the phasic and sustained components could then shift the depth and phase of the peaks.

Variations in theta-related sustained potentials with depth

Gerbrandt and Fowler[21] compared the depth distribution of DC potentials with the amplitude of the accompanying theta rhythm in CA1 and the dorsal blade of the dentate area in curarized rats. We found similar voltage vs. depth distributions in both urethane anesthetized and freely-moving rats, with an amplitude peak for both the 'DC' and the theta potentials near the hippocampal fissure. Gerbrandt and Fowler suggested a dendritic origin of both theta frequency and DC potentials mediated by entorhinal afferents. Alternatively, a glial origin of the 'DC' component is possible given the findings of high density of astroglia near the hippocampal fissure[21].

Entorhinal afferents to the dentate molecular layer seem to be able to generate sustained potentials under certain conditions. During repetitive stimulation of the perforant path, and during episodes of spreading depression after paroxysmal seizures, a sustained sink can be observed in the molecular layer, spatially corresponding to the terminal fields of the perforant path afferents (see Fig. 5 in Ref. 53). All that is required is some net tonic activity in an afferent pathway. This is possible even when individual cells of an afferent system such as the entorhinal cortex are known to fire bursts of action potentials phase-locked to the theta rhythm, since over the population of such cells some activity falls on every phase of the cycle.

Origins of sustained potentials

Some relatively small part of the sustained potentials recorded in this study could reflect inverse changes in potential with depth during non-theta EEG, since it was used as a baseline for the sustained potential recordings. It has been shown here, however, that in urethane anesthetized rats the variation with depth during non-theta is small compared to that during theta rhythm. It is reasonable, therefore, to conclude that sustained sinks and sources appear during theta rhythm and subside during non-theta EEG.

The sustained components of the hippocampal theta rhythm are large. The estimated magnitudes of sources and sinks including sustained components are up to an order of magnitude larger than the transient modulations related to the phase of the theta rhythm. The two possible cellular sources of these sustained potentials are neurons and glia.

If such sustained potentials were to be generated by glia[41], current would have to flow in a loop inward through glial cell membrane at a localized site, down the processes and outward through glial cell membrane at another site. The stimulus for such a glial current loop would presumably be a localized elevation of extracellular potassium concentration ($[K_e]$). In response to stimulation of either commissural/associational or entorhinal afferents, $[K_e]$ is higher at the somatic levels in both CA1 and dentate than at the dendritic levels and proportional to the firing rates of the cells[27]. During hippocampal theta rhythm, pyramidal cells have relatively low rates of firing, so only the dentate granule cells are likely large sources of potassium for glia. Our results indicate that the largest theta-related sustained potential generator is a sink at the hippocampal fissure. If extracellular potassium accumulation were responsible for the sustained sinks during the theta rhythm, the largest increase in $[K_e]$ would therefore be expected at the hippocampal fissure. Although Krnjevic et al.[27] showed that the potassium accumulation in dendritic regions (in association with synaptic inputs) was small relative to that in somatic regions (due to principal cell firing), we cannot completely reject the possibility that the very low firing rates of CA1 pyramidal cells during theta rhythm leads to minimal increases in $[K_e]$ at somatic levels, so emphasizing potassium accumulation at dendritic levels.

Without knowledge of changes in the extracellular distribution of potassium during theta rhythm, we favor the notion that the theta-related sustained potentials are predominantly of direct neural origin.

Sustained potentials of neural origin must arise from changes in the activity of certain hippocampal afferents during theta EEG periods relative to non-theta EEG periods. Candidate afferent populations that show such changes and are also modulated at the theta frequency include those from the septum[34,47], the retrohippocampal areas[45,48], and the ipsi- and contralateral hippocampal regions[11,17,19,38,40,44]. Candidate afferent populations that change in activity between states, but are *not* modulated at the theta frequency include those from the brainstem[52].

The rise time of the sustained components of the membrane currents is quite long, i.e. several seconds (see Fig. 1). Large sustained components of the CSD are associated with identifiable afferent populations in CA1 stratum oriens (e.g. Fig. 11, a), in the CA1 and dentate somatic layers (e.g. Fig. 11, b and f), near the hippocampal fissure (e.g. Fig. 11, d) and in the dentate mid-molecular layer (e.g. Fig. 11, e). The slow rise time of these sustained components may result from slow onsets of the changes in firing rates of afferent populations or some slow conductance changes (e.g. slow decreases in potassium conductance due to muscarinic action of acetylcholine). There is no direct evidence either for or against slow onset of changes in firing rates of *extrinsic* afferent populations. Recent observations, however, show that hippocampal interneurons can require 1 s or more to make the transition into their rhythmic, rapid, 'theta-mode' firing at the onset of theta rhythm[44]. The fact that the tonic components of the CSD generally correspond in depth with identifiable phasic components suggests that they may be produced by the same afferents causing the theta frequency components. On the other hand, slow conductance changes, caused by theta-related shifts in the firing rates of other sets of afferent populations, cannot be ruled out. The discussion in the following section relates to both the phasic and the tonic components of theta-related neural activity.

Afferents responsible for theta-related sources and sinks

Table I lists the various strata encountered along a typical electrode track through CA1 and the dentate area. For each of these strata the sources and sinks of the VHC and PP evoked potentials and the theta rhythm, and their presumed origins are summarized. For example, in CA1 stratum oriens a sink appears following VHC stimulation in all of the six profiles that included this layer. This sink reflects an EPSP from activation of commissural/associational axons of CA3/4 pyramids[1]. The peak phases and frequencies of observation are also given, both for AC and for DC theta-related CSD estimates. The theta-related sink at this level was not deeply modulated with theta phase. No prominent peak was present in the DC CSD (e.g. Fig. 11, a). With the more phase-sensitive AC analysis, a peak appeared in four of seven profiles at $324 \pm 59°$. One candidate population of afferents contributing to this sink is the set of CA3/4 pyramids that project there. Cholinergic septal afferents may also contribute to the sustained sink, but it is unlikely that their slow synaptic action on pyramids[24] could mediate theta rhythmicity. Activation of the axons of CA3 pyramids and hilar neurons by VHC stimulation also produces EPSPs in CA1 stratum radiatum[1], and in the dentate inner molecular layer[6,14]. Theta-related sinks in these two areas (e.g. Fig. 11, c2 and e) peaked at phases that were similar to the phase for the stratum oriens sink, $276 \pm 28°$ and $334 \pm 22°$, respectively, so these populations may produce the phasic component of all three sinks. The low firing rates of CA3/4 pyramids during theta rhythm[17] make it unlikely that they are producing the relatively large sustained component of the sink in CA1 stratum oriens. This may be produced by activity in some subcortical site. Alternatively, the sustained CA1 basal sink may be passively related to active sources at the level of the cell bodies of the pyramidal cells. However, the fact that a basal sink appears in theta rhythm under urethane anesthesia in the absence of a prominent somatic source argues against the passive interpretation.

Recordings of CA3/4 pyramidal cell firing in walking rats showed different phases in different laboratories. In this laboratory, average peak phase was reported to be 19°[19], while Buzsáki et al.[11] found them to fire at about 270°. The latter data fit with the phase of the sinks in strata oriens and radiatum better than do those from this laboratory. The explanation may involve changes in preferred phase of firing related to changes in the firing rate of pyramidal cells. Hippocampal pyramidal cells have been observed to advance their phase of firing with respect to the theta rhythm by more than 110° with changes in firing rate from $< 1/s$ to $> 10/s$ (Fox, unpublished observations), bringing them more in line with the data of Buzsáki et al.[11]. The high firing rates were observed in the 'place field' of the cell and the low rates outside this field[28]. All of the data from Fox et al.[19] were recorded from slowly firing cells during treadmill walking. More rapid firing of these afferents would be more likely to appear near 270° and would produce greater temporal summation of CSD components than slow firing. Another

possible explanation of the better correspondence of the phasic component of the commissural/associational sinks with the cellular data of Buzsáki, et al.[11] are differences in the frequency of the theta rhythm related to the behavioral task. In these experiments the running wheel task was very similar to that used by Buzsáki et al. In the Fox et al.[19] experiments, the rats walked on a treadmill. The frequency of the theta rhythm during running on a wheel for water reward is generally higher than during forced locomotion on a treadmill (Fox, unpublished observations).

At the level of the cell bodies of the CA1 pyramids is a theta-related source (e.g. Fig. 11, b). This source is mainly tonic. It may reflect increased activity of inhibitory interneurons during theta rhythm[17]. The phasic component of this source is relatively small. There has been some controversy about the phase of firing of CA1 interneurons. Sinclair et al.[40] and Fox et al.[19] found them firing predominantly near the positive peak of the dentate theta wave. Buzsáki et al.[11] found them near the negative peak, but both Fox et al.[19] and Buzsáki et al.[11] found some cells firing on the phase opposite to their dominant group. There may be two populations of such cells with microelectrode sampling biases determining which population is recorded. In the granule cells, long duration increases in somatic K^+ currents resulting from increased rate of firing during theta rhythm[38], in addition to recurrent IPSPs, may contribute to the somatic source (e.g. Fig. 11, f). A predominantly sustained sink appears in proximal stratum radiatum of CA1 (e.g. Fig. 11, c1). Minimally, a component of this sink is passively related to the somatic source. The absence of both this sink and the somatic source under urethane suggests that they are related. Perhaps the proximal radiatum sink is entirely passive; it is unclear what afferents could cause a large active sustained sink localized to this depth.

Afferents from the lateral entorhinal cortex project to the distal apical dendrites of both CA1 pyramids and dentate granule cells[42]. They may be producing the sinks in stratum lacunosum-moleculare of CA1 and the distal molecular layer of the dentate (e.g. Fig. 11, d). The former sink peaks at $129 \pm 31°$ and the latter peaks at $158 \pm 39°$. In urethane-anesthetized rats there is a large sink near the fissure peaking on a similar phase of the theta rhythm. The four lateral entorhinal units recorded thus far in urethane anesthetized rats have phase histograms that peak at $134 \pm 27°$[45]. Activity in these lateral entorhinal afferents may be partly responsible for the phasic modulation of excitability of CA1 pyramidal cells and dentate granule cells as tested by VHC and PP stimulation, respectively[39]. The lack of firing of many of the CA1 inhibitory interneurons on the negative phase[19,40] may also contribute. Peak excitability occurred at 110° for both areas in walking rats.

Afferents from the medial entorhinal cortex project to the distal apical dendrites of CA1 pyramids and the middle part of the dentate molecular layer[42]. The peak theta-related firing of medial entorhinal neurons in walking rats occurs at $5 \pm 47°$ after the negative peak of the CA1 theta rhythm[48]. The positive peak of the dentate theta rhythm that is used as a reference here occurs about 45 degrees after the CA1 negative peak due to the incomplete phase reversal between CA1 and the hippocampal fissure (see Fig. 9). Thus we can estimate that the peak firing of medial entorhinal afferents in walking rats occurs at about 320° after the positive peak of the dentate theta. This is close to the phase of the peak of the sink in the dentate middle molecular layer ($260 \pm 26°$) in rats running on a wheel (e.g. Fig. 11, e). This is also close to the peak phase of firing of the dentate granule cells (296°), the CA3/4 pyramidal cells (described above), the CA3/4 interneurons (310°), the CA1 pyramidal cells (325°), and the CA1 interneurons (310°)[19] in walking rats. It appears that the medial entorhinal cortex (MEC) input strongly influences the dentate granule cells, due to its relative proximity to the soma compared to the lateral entorhinal cortex input. The granule cells drive the theta-related firing of CA3/4 pyramids and interneurons, and the CA3/4 pyramids, in turn, drive the CA1 pyramids and interneurons. These relationships do not appear to hold for urethane-anesthetized rats. It is not even clear that there is a mid-molecular sink, the more proximal dentate molecular layer sink in Fig. 5D may be in the inner molecular layer. The peak phases of the

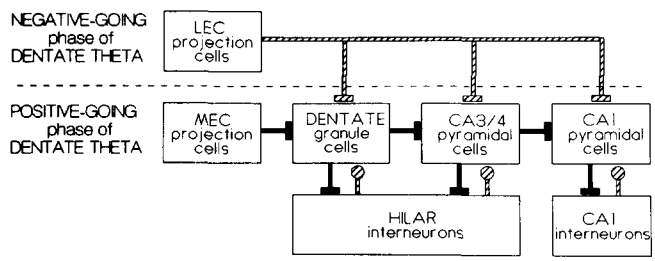

Fig. 12. Intrinsic connections of the hippocampal formation generating the theta rhythm during running. Synaptic inputs that provide strong phasic modulation of the firing of postsynaptic neurons are indicated by solid connections. Synaptic inputs that generate membrane current contributing to the field potentials, but do not strongly modulate the phasic firing of postsynaptic neurons are indicated by hatched connections. Excitatory interactions are indicated by straight bars at the end of connections, inhibitory interactions by circles. Cells that fire and produce sinks on the negative-going phase of dentate theta rhythm appear above the dashed line. Cells that fire and produce sinks on the positive-going phase appear below the dashed line. LEC, lateral entorhinal cortex; MEC, medial entorhinal cortex.

MEC firing (90°[48]) and the moleculare sink (300°), and the granule cell firing (183°[19]) do not correspond.

The above relationships for movement-related theta rhythm are summarized in Fig. 12. Cell populations that fire predominantly on the positive-going phase of the dentate theta rhythm are indicated below the horizontal dashed line; the lateral entorhinal cortex (LEC) projection cells are indicated above the line to indicate that they fire on the negative-going phase. Excitatory interactions are indicated by straight bars at the end of connections, inhibitory interactions by circles. Strong synaptic effects that drive the firing of the postsynaptic population are indicated by solid connections, weak ones by hatched connections. The weak excitatory and inhibitory connections generate membrane currents that contribute to CSD, but do not strongly affect the phase of firing of the cells. MEC also projects directly to the distal dendrites of the pyramidal cells of Ammon's horn[42] in addition to the illustrated projections to the dentate granule cells. These connections were omitted from the Fig. because the theta-related CSD in stratum lacunosum-moleculare of CA1 appears to be dominated by the effects of the LEC afferents. The weak excitation of distal dendrites of granule and pyramidal cells at the fissure generates a large extracellular sink that is responsible for much of the amplitude of the AC component of the theta rhythm, but it has little effect on firing probability because its effects are overcome by more proximally placed afferents. Rhythmic cholinergic neurons in the medial septal nucleus and the nucleus of the diagonal band may organize the rhythmic oscillation of medial entorhinal cells at the theta frequency by rapid muscarinic excitation of interneurons in a manner similar to their proposed effect in the hippocampus[36,47,49].

This paper has demonstrated: (1) that it is possible to eliminate false generators and improve quantitative estimates of current source density for continuous processes like the EEG by using DC-coupled amplifiers; (2) that the difference in DC between theta and non-theta EEG periods is sufficient for current source density analysis of the theta rhythm that occurs during wheel-running; (3) that CSD profiles including the sustained components are consistent across rats running on a wheel; and (4) that it is possible in most cases to relate real generators of membrane current to known afferent populations with known firing relations to the theta rhythm. Firmly establishing the identity of the afferents responsible for the generation of the phasic and tonic components of the theta-related CSD will lead to a better understanding of the sequence of activity within the septohippocampal and related neural circuitry during theta rhythm.

Acknowledgements. The authors thank Mrs. S. Brankatschk for the histology and Dr. J.B. Ranck Jr, and Dr. R.U. Muller for helpful discussions. Supported by National Institutes of Health Grants NS17095 (to S.E.F.), NS09175 (to M.S.), and NS07117 (Institutional Neurophysiology training grant).

REFERENCES

1 Andersen, P., Interhippocampal impulses. II. Apical dendritic activation of CA1 neurons, *Acta Physiol. Scand.*, 48 (1960) 178–208.
2 Andersen, P., Bliss, T.V.P. and Skrede, K.K., Unit analysis of hippocampal population spikes, *Exp. Brain Res.*, 13 (1971) 208–221.
3 Andersen, P., Eccles, J.C. and Loyning, Y., Location of postsynaptic inhibitory synapses on hippocampal pyramids, *J. Neurophysiol.*, 27 (1964) 592–607.
4 Andersen, P., Holmqvist, B. and Voorhoeve, P.E., Entorhinal activation of dentate granule cells, *Acta Physiol Scand.*, 66 (1966) 448–460.
5 Andersen, P., Holmqvist, B. and Voorhoeve, P.E., Excitatory synapses on hippocampal apical dendrites activated by entorhinal stimulation, *Acta Physiol Scand.*, 66 (1966) 461–472.
6 Berger, T.W., Semple-Rowland, S. and Bassett, J.L., Hippocampal polymorph neurons are the cells of origin for ipsilateral association and commissural afferents to the dentate gyrus, *Brain Res.*, 215 (1981) 329–336.
7 Bland, B.H. and Whishaw, I.Q., Generators and topography of hippocampal theta (RSA) in the anesthetized and freely-moving rat, *Brain Res.*, 118 (1976) 259–280.
8 Brankačk, J. and Fox, S.E., Current sources for the alternating and sustained potentials of the hippocampal theta rhythms of the rat, *Soc. Neurosci. Abstr.*, 13 (1987) 1331.
9 Buzsáki, G., Feed-forward inhibition in the hippocampal formation, *Prog. Neurobiol.*, 22 (1984) 131–153.
10 Buzsáki, G., Czopf, J., Kondakor, I. and Kellenyi, L., Laminar distribution of hippocampal rhythmic slow activity (RSA) in the behaving rat: current-source density analysis, effects of urethane and atropine, *Brain Res.*, 365 (1986) 125–137.
11 Buzsáki, G., Leung, L.W.S. and Vanderwolf, C.H., Cellular bases of hippocampal EEG in the behaving rat, *Brain Res. Rev.*, 6 (1983) 139–171.
12 Caspers, H., Speckmann, E-J. and Lehmenkuhler, A., Electrogenesis of slow potentials in the brain. In T. Elbert, B. Rockstroh, W. Lutzenberger and N. Birbaumer (Eds.) *Self-regulation of the Brain and Behavior*, Springer, Berlin, 1984, pp. 27–41.
13 Deadwyler, S.A., West, J.R., Cotman, C.W. and Lynch, G., Physiological studies of the reciprocal connections between the hippocampus and the entorhinal cortex, *Exp. Neurol.*, 49 (1975) 35–57.
14 Deadwyler, S.A., West, J.R., Cotman, C.W. and Lynch, G.S., A neurophysiological analysis of the commissural projections to the dentate gyrus of the rat, *J. Neurophysiol.*, 38 (1975) 164–184.
15 Doller, H.J. and Weight, F.F., Perforant pathway activation of hippocampal CA1 stratum pyramidale neurons: electrophysiological evidence for a direct pathway, *Brain Res.*, 237 (1982) 1–13.
16 Etlinger, S.C., Guttmann, G. and Bauer, H., Spontaneous cortical DC-potential shifts: modulation stereotypy; relationships to higher EEG-frequencies, *Int. J. Psychophysiol.*, 4 (1986) 121–128.
17 Fox, S.E. and Ranck Jr., J.B., Electrophysiological characteristics of hippocampal complex-spike cells and theta cells, *Exp. Brain Res.*, 41 (1981) 399–410.
18 Fox, S.E. and Stewart, M., Analysis of hippocampal theta rhythm shows that correct location of current sources and sinks generating EEG patterns can require DC recording, *Soc. Neurosci. Abstr.*, 12 (1986) 1527.
19 Fox, S.E., Wolfson, S. and Ranck Jr., J.B., Hippocampal theta rhythm and the firing of neurons in walking and urethane-anesthetized rats, *Exp. Brain Res.*, 62 (1986) 495–508.
20 Freeman, J.A. and Nicholson, C., Experimental optimization of

current source-density technique for anuran cerebellum, *J. Neurophysiol.*, 38 (1975) 369–382.
21 Gerbrandt, L.K. and Fowler, J.R., Arousal-related sustained potentials in neocortex and hippocampus of rats, *Prog. Brain Res.*, 54 (1980) 109–116.
22 Gottlieb, D.I. and Cowan, W.M., Autoradiographic studies of the commissural and ipsilateral associational connections of the hippocampus and dentate gyrus of the rat. I. The commissural connection, *J. Comp. Neurol.*, 149 (1973) 393–422.
23 Green, K.F. and Rawlins, J.N.P., Hippocampal theta in rats under urethane: generators and phase relations, *Electroencephalogr. Clin. Neurophysiol.*, 47 (1979) 420–429.
24 Halliwell, J.V. and Adams, P.R., Voltage-clamp analysis of muscarinic excitation in hippocampal neurons, *Brain Res.*, 250 (1982) 71–92.
25 Holsheimer, J., Electrical conductivity of the hippocampal CA1 layers and application to current source density analysis, *Exp. Brain Res.*, 67 (1987) 402–410.
26 Jackson, D.E. and O'Dell, J.W., The VIC-20 computer and an interface system for controlling operant chambers, *Behav. Res. Meth. Instrum. Comput.*, 17 (1985) 406–408.
27 Krnjevic, K., Morris, M.E., Reiffenstein, R.J. and Ropert, N., Depth distribution and mechanism of changes in extracellular K^+ and Ca^{2+} concentrations in the hippocampus, *Can. J. Physiol. Pharmacol.*, 60 (1982) 1658–1671.
28 Kubie, J.L., Muller, R.U. and Fox, S.E., Firing fields of hippocampal place cells: interim report. In G. Buzsáki and C.H. Vanderwolf (Eds.) *Electrical Activity of the Archicortex*, Hungarian Academy of Sciences, Budapest, 1985, pp. 221–231.
29 Lomo, T., Patterns of activation in a monosynaptic cortical pathway: the perforant path input to the dentate area of the hippocampal formation, *Exp. Brain Res.*, 12 (1971) 18–45.
30 Lopes da Silva, F.H., Witter, M.P., Boeijinga, P.H. and Lohman, A.H.M., Anatomic organization and physiology of the limbic cortex, *Physiol. Rev.*, 70 (1990) 453–512.
31 Nicholson, C. and Freeman, J.A., Theory of current source-density analysis and determination of conductivity tensor for anuran cerebellum, *J. Neurophysiol.*, 38 (1975) 356–368.
32 O'Leary, J.L. and Goldring, S., DC potentials of the brain, *Physiol. Rev.*, 44 (1964) 91–125.
33 Paxinos, G. and Watson, C., *The Rat Brain in Stereotaxic Coordinates*, Academic Press, Sydney, 1982.
34 Petsche, H., Stumpf, Ch. and Gogolak, G., The significance of the rabbit's septum as a relay station between the midbrain and the hippocampus I. The control of hippocampus arousal activity by the septum cells, *Electroencephalogr. Clin. Neurophysiol.*, 14 (1962) 202–211.
35 Ranck Jr., J.B., Specific impedance of rabbit cerebral cortex, *Exp. Neurol.*, 7 (1963) 144–152.
36 Reece, L.J. and Schwartzkroin, P.A., Effects of cholinergic agonists on two non-pyramidal cell types in rat hippocampal slices, *Brain Res.*, 566 (1991) 115–126.
37 Robinson, T.E., Hippocampal rhythmic slow activity (RSA; theta): a critical analysis of selected studies and discussion of possible species-differences, *Brain Res. Rev.*, 2 (1980) 69–101.
38 Rose, G., Diamond, D. and Lynch, G.S., Dentate granule cells in the rat hippocampal formation have the behavioral characteristics of theta neurons, *Brain Res.*, 266 (1983) 29–37.
39 Rudell, A.P., Fox, S.E. and Ranck Jr., J.B., Hippocampal excitability phase-locked to the theta rhythm in walking rats, *Exp. Neurol.*, 68 (1980) 87–96.
40 Sinclair, B.R., Seto, M.G. and Bland, B.H., Theta-cells in CA1 and dentate layers of hippocampal formation: relations to slow wave activity and motor behavior in the freely-moving rat, *J. Neurophysiol.*, 48 (1982) 1214–1225.
41 Somjen, G.G., Electrophysiology of Neuroglia, *Annu. Rev. Physiol.*, 37 (1975) 163–190.
42 Steward, O., Topographic organization of the projections from the entorhinal area to the hippocampal formation of the rat, *J. Comp. Neurol.*, 167 (1976) 285–314.
43 Steward, O. and Scoville, S.A., Cells of origin of entorhinal cortical afferents to the hippocampus and fascia dentata of the rat, *J. Comp. Neurol.*, 167 (1976) 285–314.
44 Stewart, M., Disinhibition of hippocampal pyramidal cells during the transition into theta rhythm, *Exp. Brain Res.*, in press.
45 Stewart, M., Barry, M., Quirk, G.J. and Fox, S.E., Firing relations of entorhinal neurons to the hippocampal theta rhythm in walking and urethane anesthetized rats, *Soc. Neurosci. Abstr.*, 17 (1991) 1036.
46 Stewart, M. and Fox, S.E., Two populations of rhythmically bursting neurons in rat medial septum are revealed by atropine, *J. Neurophysiol.*, 61 (1989) 982–993.
47 Stewart, M. and Fox, S.E., Do septal neurons pace the hippocampal theta rhythm? *Trends in Neurosci.*, 13 (1990) 163–168.
48 Stewart, M., Quirk, G.J., Barry, M. and Fox, S.E., Firing relations of medial entorhinal neurons to the hippocampal theta rhythm in urethane-anesthetized and walking rats, *Exp. Brain Res.*, 90 (1992) 21–28.
49 Van der Zee, E.A., De Jong, G.I., Strosberg, A.D. and Luiten, P.G.M., Parvalbumin-positive neurons in rat dorsal hippocampus contain muscarinic acetylcholine receptors, *Brain Res. Bull.*, 27 (1991) 697–700.
50 Vanderwolf, C.H., Hippocampal electrical activity and voluntary movement in the rat, *Electroencephalogr. Clin. Neurophysiol.*, 26 (1969) 407–418.
51 Vanderwolf, C.H., Cerebral activity and behavior: control by central cholinergic and serotonergic systems, *Int. Rev. Neurobiol.*, 30 (1988) 225–340.
52 Vertes, R.P., Brainstem gigantocellular neurons: patterns of activity during behavior and sleep in the freely-moving rat, *J. Neurophysiol.*, 42 (1979) 214–228.
53 Wadman, W.J., Juta, A.J.A., Kamphuis, W. and Somjen, G.G., Current source density of sustained potential shifts associated with electrographic seizures and with spreading depression in rat hippocampus, *Brain Res.*, 570 (1992) 85–91.
54 Winson, J., Patterns of hippocampal theta rhythm in the freely-moving rat, *Electroencephalogr. Clin. Neurophysiol.*, 36 (1974) 291–301.
55 Yeckel, M.F. and Berger, T.W., Feedforward excitation of the hippocampus by afferents from the entorhinal cortex: redefinition of the role of the trisynaptic pathway, *Proc. Natl. Acad. Sci. USA*, 87 (1990) 5832–5836.